Optical Engineering

OpticalEngineering.SPIEDigitalLibrary.org

Subsurface mechanical damage correlations after grinding of various optical materials

Tayyab I. Suratwala
William A. Steele
Lana L. Wong
Gary C. Tham
Joel F. Destino
Philip E. Miller
Nathan J. Ray
Joseph A. Menapace
Eyal Feigenbaum
Nan Shen
Michael D. Feit

SPIE.

Tayyab I. Suratwala, William A. Steele, Lana L. Wong, Gary C. Tham, Joel F. Destino, Philip E. Miller, Nathan J. Ray, Joseph A. Menapace, Eyal Feigenbaum, Nan Shen, Michael D. Feit, "Subsurface mechanical damage correlations after grinding of various optical materials," *Opt. Eng.* **58**(9), 092604 (2019), doi: 10.1117/1.OE.58.9.092604.

Subsurface mechanical damage correlations after grinding of various optical materials

Tayyab I. Suratwala,[a,*] William A. Steele,[a] Lana L. Wong,[a] Gary C. Tham,[a] Joel F. Destino,[b] Philip E. Miller,[a] Nathan J. Ray,[a] Joseph A. Menapace,[a] Eyal Feigenbaum,[a] Nan Shen,[a] and Michael D. Feit[a]

[a]Lawrence Livermore National Laboratory, Livermore, California, United States
[b]Creighton University, Omaha, Nebraska, United States

Abstract. Loose abrasive grinding was performed on a wide range of optical workpiece materials [single crystals of Al_2O_3 (sapphire), SiC, $Y_3Al_5O_{12}$ (YAG), CaF_2, and LiB_3O_5 (LBO); a SiO_2-Al_2O_3-P_2O_5-Li_2O glass-ceramic (Zerodur); and glasses of SiO_2:TiO_2 (ULE), SiO_2 (fused silica), and P_2O_5-Al_2O_3-K_2O-BaO (phosphate)]. Using the magneto rheological finishing (MRF) taper wedge technique (where a wedge was polished on each of the ground workpieces and the resulting samples were appropriately chemically etched), the subsurface mechanical damage (SSD) characteristics were measured. The SSD depth for most of the workpiece materials was found to scale as $E_1^{1/2}/H_1$, where E_1 is the elastic modulus and H_1 is the hardness of the workpiece. This material scaling is the same as that for the growth of lateral cracks, suggesting that lateral cracks are a dominant source for SSD rather than radial/median cracks, as previously proposed. Utilizing the SSD depth data from both this study and others, semiempirical relationships have been formulated, which allows for estimating the SSD depth as a function of workpiece material and important grinding parameters (such as abrasive size and applied pressure). [DOI: 10.1117/1.OE.58.9.092604]

Keywords: optical materials; grinding, lateral cracks; subsurface damage; glass; single crystals; optical fabrication.

Paper 190086SS received Jan. 20, 2019; accepted for publication Mar. 26, 2019; published online Apr. 25, 2019.

1 Introduction

The grinding of brittle materials can be described microscopically as the removal of workpiece particles created from an ensemble of single or intersecting brittle fractures, which are caused by an ensemble of normally loaded, hard indenters or abrasives sliding or rolling across the surface of the workpiece. These microfractures result in the desired outcome of removing material from the surface to shape the workpiece; however, this occurs at the expense of leaving behind subsurface mechanical damage (SSD) that needs to be removed during the subsequent fabrication process steps. In the case of optical components, SSD on the final fabricated optic has been shown to negatively influence its performance (e.g., increasing optical scatter, reducing mechanical strength, and increasing laser damage). Hence understanding the mechanism of SSD creation and predicting the SSD depth has the practical payoff of enabling the development of optical fabrication processes, which minimize and potentially eliminate SSD and therefore lead to the manufacturing of optics both more economically and with better performance.

SSD created during grinding and polishing has been a topic of much study, both in terms of methods to measure as well as to understand its creation.[1,2] The influence of various grinding parameters, such as abrasive size, depth of cut, and applied pressure, has been investigated. However, due to the complex set of interactions occurring at the workpiece–lap interface, the development of a global quantitative model for grinding SSD has been challenging to develop. Some of these interactions include: (1) the agglomeration, comminution, and/or rotation of the abrasive particles; (2) the presence of rogue particles; and (3) the complex load distribution on the abrasive particles due to its particle size distribution as well as the mechanical properties and surface topology of the workpiece and lap.

In this study, we attempt to lean toward a more global grinding SSD damage model. First, one important parameter not systematically evaluated to date with respect to SSD is the influence of workpiece properties on the SSD depth characteristics. Hence, in this study, the SSD correlations among a wide variety of workpiece materials are evaluated and implications on the mechanisms of SSD creation are described. Second, using SSD data from previous studies, more global semiempirical SSD correlations are developed to estimate SSD depth as a function of various workpiece materials as well as important grinding process parameters (such as, abrasive size and applied pressure). The workpiece materials utilized in this study have also been used as part of a broader study to develop more predictive quantitative relationships during optical fabrication (such as polishing removal rate, grinding removal rate, and grinding surface roughness as a function of workpiece materials) with the aim to enable accelerated development of optical fabrication processes for new workpiece materials.[3,4]

2 Experimental

2.1 *Optical Material Workpieces*

Nine different optical workpiece materials were utilized for the grinding experiments: single crystal Al_2O_3 (sapphire) (a-plane, Coastline Optics, Camarillo, California), single crystal SiC (SiC-6H 0001, MTI Corporation, Richmond, California), single crystal $Y_3Al_5O_{12}$ (YAG) (Northrop

*Address all correspondence to Tayyab I. Suratwala, E-mail: suratwala1@llnl.gov

0091-3286/2019/$28.00

Grumman/Synoptics, Charlotte, North Carolina), single crystal CaF_2 (111 orientation, ISP, Irvington, New York), single crystal LiB_3O_5 (LBO) (2ω doubler cut, Coherent Crystal, New Jersey), SiO_2-Al_2O_3-P_2O_5-Li_2O glass ceramic (Zerodur) (Schott, Duryea, Pennsylvania), SiO_2:TiO_2 glass (ULE) (Corning Inc., Corning, New York), SiO_2 glass (Fused Silica) (Corning 7980, Corning Inc., Corning, New York), and P_2O_5-Al_2O_3-K_2O-BaO glass (phosphate glass) (LHG-8, Hoya Corporation, Milpitas, California). All the samples were 50 mm in diameter and typically 1 cm thick.

2.2 *Grinding Experiments*

Loose abrasive grinding of each of the workpiece materials was conducted on a 300-mm-diameter flat granite lap utilizing 15-μm Al_2O_3 abrasives (Microgrit WCA 15T; Universal Photonics, Hicksville, New York). The loose abrasive slurry was prepared as five parts water to one part abrasive powder and fed single pass with a 1.2-mL/min feed rate using a peristaltic pump. The same grinding conditions were used for each of the workpieces, namely: lap rotation of 20 rpm, workpiece rotation of 20 rpm, center offset between workpiece and lap center of 75 mm, and applied pressure on workpiece of 1.1 psi using weights on the workpiece.

2.3 *SSD Measurement*

The SSD depth and length distributions for each of the workpieces were measured using the magneto rheological finishing (MRF) taper wedge technique. The details of this process are described elsewhere.[5,6] Figure 1 schematically illustrates the process. After grinding, each workpiece was polished using MRF (QED 22Y, QED, Rochester, New York) using either a cerium oxide-based slurry (C10+) or diamond-based (D10) slurry on a 50-mm MRF wheel using 2751 rpm pump speed and an 18-Amp field intensity. A shallow one-dimensional linear wedge was created ranging in maximum depth from 11 to 150 μm (depending on the amount of SSD observed on a given workpiece) over an area of 20 mm $\times$ 30 mm on the workpiece surface. Each of the optical workpieces was then chemically etched $\sim$1 μm; the specific etch process and chemistry are described for each of the workpiece materials in Table 1. Next, the polished portion of each workpiece material was characterized by optical microscopy to view the exposed SSD cracks at various polished depths along the MRF wedge. For the SSD depth distribution, the obscuration of the cracks on the surface, which is proportional to the number density of cracks, as a function of depth into the surface was determined. The crack obscuration was determined via image analysis (by image thresholding and calculating the area of cracks in the field of view) of each of the optical microscopy images along the wedge (corresponding to depth into the workpiece). Note, at low obscurations, multiple images at a given depth were analyzed for improved statistics. For the SSD length distribution, the cumulative distribution of only isolated (not intersecting) crack lengths on the surface at all depths along the wedge combined was determined.

3 Results

A photo of each of the workpiece materials after being ground and polished with a wedge is shown in Fig. 2. Table 1 summarizes the list of workpiece materials evaluated, their relevant material properties, etching parameters, MRF wedge parameters, and the measured SSD results. Chemical etching was performed on each of the wedged workpiece materials in order to reveal any hidden SSD from the surface.[7] Because of the broad range of material types (glasses, single crystals, and glass–ceramics) and material chemistries, a unique etch recipe (composition, concentration, temperature, and etch time) had to be developed in order to practically etch $\sim$1 μm from the workpiece surface. The details of the etch recipes for each workpiece material are described in Table 1. The etching composition varied dramatically such as: buffered oxide etch (NH_4F:HF) for the silica-based glasses or glass-ceramics; concentrated base (sodium hydroxide) for the phosphate glass; acetic acid for LBO; hydrochloric acid for CaF_2; concentrated potassium hydroxide at elevated temperatures for SiC; and more complex recipes using concentrated sulfuric/phosphoric acid, often at elevated temperatures, followed by a sulfuric acid rinse for the sapphire and YAG single crystals. Successful etching resulted in the exposure of SSD as shown in Fig. 3(a). However, unoptimized etching can easily lead to problems such as thermal fracture during elevated temperature etching followed by lower temperature rinsing [see Fig. 3(b)], anisotropic etching at crystal dislocations [see Fig. 3(c)], and/or redeposition of etch by-products on the workpiece surface [see Fig. 3(d)]. These issues were largely resolved by choosing etch recipes that had elevated temperature rinsing that was slowly ramped down to room temperature reducing the driving force for thermal fracture, slowing down the etch rate to minimize the effect of revealing etched dislocations, and slowing down the etch rate combined with aggressive rinsing to minimize redeposition.

Figure 4 shows example microscope images at fixed depths of 5, 7, and 13 μm along the polished wedge of the ground surfaces for each of the workpieces. The character of the individual microcracks is similar for all the workpieces as observed in previous studies (for example, see Ref. 6); the width of the microcrack is determined by the amount etched

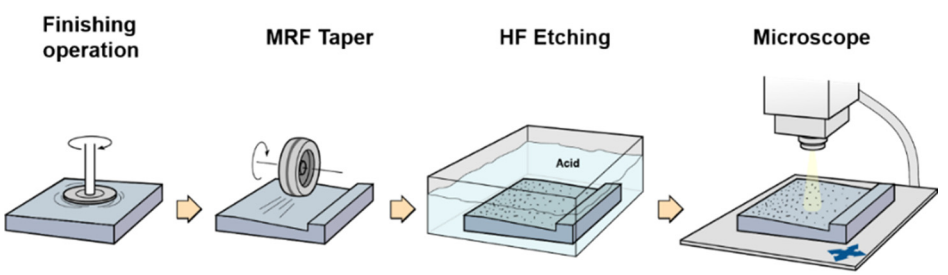

Fig. 1 Schematic illustration of the MRF wedge techniques utilized for measured SSD characteristics. (after Refs. 5, 6.)

Table 1 List of workpiece materials, basic material properties, etching parameters, MRF wedge parameters, and SSD results.

			Workpiece material properties			Etching process				MRF wedge SSD				
Work piece material	Composition	Material type	Young's modulus, E_1 (GPa)	Knoop hardness, H_1 (GPa)	Fracture toughness, K_{Ic} (MPa.m$^{0.5}$)	Etch recipe	Temperature (°C)	Etch rate (μm/h)	Etch time (h)	MRF slurry	Wedge depth (μm)	SSD depth 10^{-4} Obs (μm)	SSD depth 10^{-5} Obs (μm)	SSD average length (μm)
Sapphire	Al_2O_3	Single crystal	345	17.2	3.45	H_2SO_4: $H_3PO_4$3:1; H_2SO_4	260	1.2	0.3	NA	NA	0	0	NA
Silicon carbide	SiC	Single crystal	410	27.5	4.6	KOH	480	30	NA	NA	NA	0	0	NA
YAG	$Y_3Al_5O_{12}$	Single crystal	300	11.9	2	H_2SO_4: $H_3PO_4$3:1; H_2SO_4	22	0.03	20.0	D10	40	11.2	20.0	4.5
Calcium fluoride	CaF_2	Single crystal	76	1.5	0.55	2.5M HCl	22	3.0	0.3	C10+	53	15.1	18.3	12.6
LBO	LiB_3O_5	Single crystal	140	6.0	0.54	0.2M CH_3COOH	22	3.0	0.3	C10+	91	18.0	22.3	14.3
Zerodur	SiO_2:Al_2O_3: P_2O_5:Li_2O	Glass-ceramic	90.3	6.1	0.9	NH_4F:HF 6:1 (3× diluted)	22	1.0	1.0	C10+	150	12.5	15.9	10.3
ULE	SiO_2:TiO_2	Glass	68	4.3	1.43	NH_4F:HF 6:1 (10× diluted)	22	3.0	0.3	C10+	36	24.6	27.7	13.5
Fused silica	SiO_2	Glass	72.7	5.9	0.75	NH_4F:HF 6:1 (3× diluted)	22	1.6	0.7	C10+	15	7.5	7.6	11.9
Phosphate	P_2O_5:Al_2O_3: K_2O:BaO	Glass	50	3.2	0.51	2M NaOH	22	0.8	1.3	C10+	73	30.6	39.4	9.8

NA, not applicable.

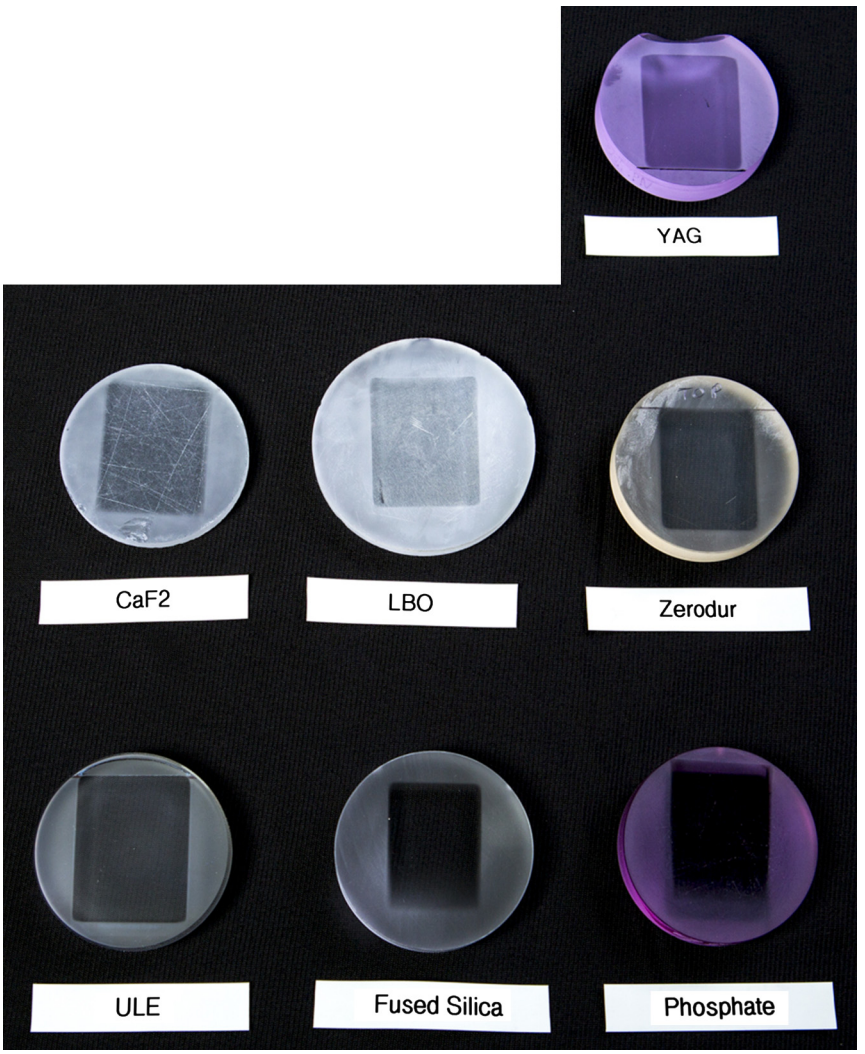

Fig. 2 Photo of the various optical workpiece materials after being ground using a 15-μm Al_2O_3 loose abrasive and processing the MRF polished wedge.

and length is determined by the grinding process and workpiece material. The relative areal amount of SSD can be easily visually compared in Fig. 4 by ranking the degree of obscuration (i.e., amount of total crack area in the field of view of the image) at a fixed depth. Hence, phosphate glass clearly had the largest amount of SSD damage, whereas YAG and fused silica had the least amount of SSD damage.

Figure 5 shows the SSD depth distribution in terms of obscuration (which is proportional to crack number density) as a function of depth for all the workpiece materials characterized in this study after grinding with the same 15-μm Al_2O_3 process. Note the plot is on a semilog scale with the obscuration spanning up to six-orders-of-magnitude. The magnitudes of the SSD depth, arbitrarily defined at an obscuration of 10^{-4} or 10^{-5}, are summarized in Table 1. Consistent with the visual observations from Fig. 4, fused silica and YAG had the least amount of SSD depth, and phosphate glass had the deepest SSD.

Similarly, Fig. 6(a) shows the crack length distributions for the same samples but presented as cumulative fraction of analyzed individual cracks. Again, the average crack length for each of the workpieces is summarized in Table 1. Most of the workpieces had similar crack length distributions, except for YAG and LBO. Comparing the average crack length from this study with our previous study Ref. 6, the dominant factor controlling the crack length is the abrasive size rather than the mechanical properties of the workpiece material [see Fig. 6(b)].

Note the 15-μm Al_2O_3 grinding process did not remove material from SiC and Sapphire, and hence its SSD is reported as zero (see Table 1) and excluded from Figs. 4–6.

4 Discussion

4.1 *Correlation Between SSD Depth and Workpiece Material Properties*

A key objective of the present study is to determine how basic material properties of the workpiece influence the SSD during grinding. Here, we compare how the SSD depth scales with material scaling factors for basic types of cracks created on the surface. The dominant factors that determine the depth of the cracks during sharp indentation are the mechanical properties of the workpiece and the applied normal load. The relationships that govern the extent

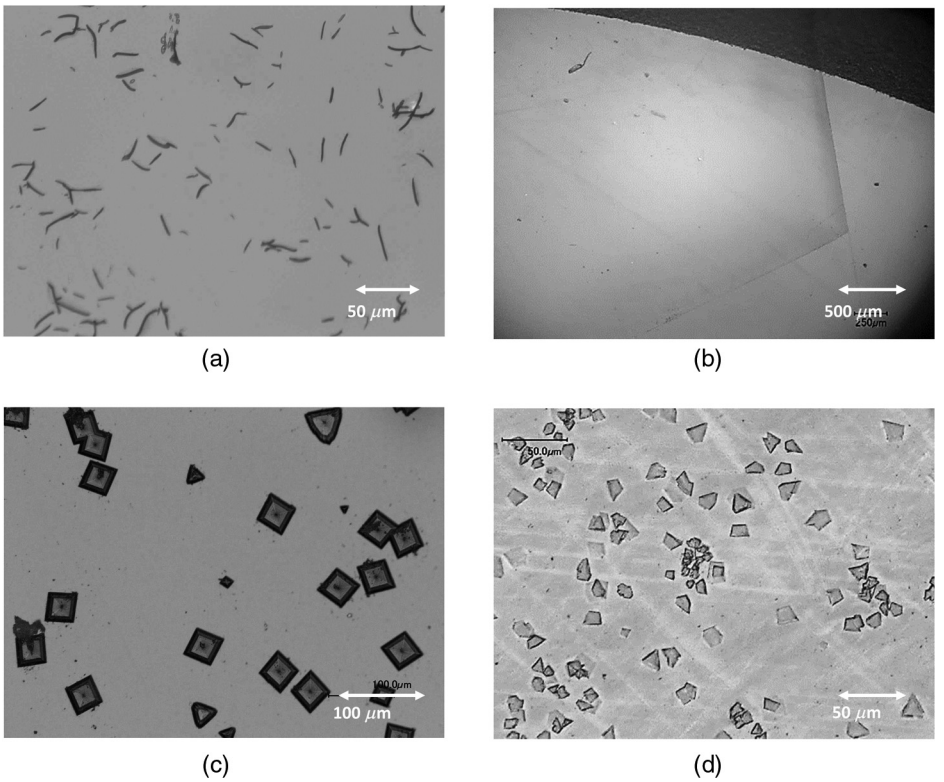

Fig. 3 Optical micrographs of the optical workpiece surfaces after chemical etching illustrating: (a) revealing the SSD fractures on fused silica (desired); (b) thermal fracture on sapphire (undesired); (c) revealing dislocations on sapphire (undesired); and (d) redeposition on Zerodur (undesired).

of radial and lateral fracture growth, in isotropic materials following crack initiation, as a function of applied load (P) are given by[8–10]

$$c_r = s_r P^{2/3}, \tag{1a}$$

$$c_\ell = s_\ell P^{1/2}, \tag{1b}$$

where c_r and c_ℓ are the crack depths (μm), and s_r and s_ℓ are the rates of crack growth with scaled load (referred to as crack slope). The subscripts r and ℓ designate radial and lateral cracks, respectively. In a previous study, we measured both the lateral and radial crack depths as a function of the applied load on the same set of optical workpiece materials utilized in this study.[11] The load dependence was largely consistent with that described in Eqs. (1a) and (1b); the rate of increase in crack depth as a function of scaled load (s_r or s_ℓ) was determined. The growth rate of the crack is known to scale with the material properties of the workpiece, namely ${E_1}^{1/2}/H_1$ for lateral cracks and $(E_1/H_1{K_{Ic}}^2)^{1/3}$ for radial cracks.[1,11,12] Because lateral cracks tend to propagate parallel to the workpiece surface and often break to the surface, they are more inclined to release a chip of the workpiece material. Hence lateral cracks are known to be the dominant crack type leading to material removal, and have been shown to scale with grinding rate and grinding surface roughness.[1,11–13] By the same reasoning, because radial/median cracks propagate perpendicular to the workpiece surface, they have been thought to be the dominant crack type governing SSD depth.[6]

Figures 7(a) and 7(b) show how well the measured SSD depth for a fixed grinding process scales with both the lateral crack and radial crack material scaling factors. Surprisingly, SSD depth was found to scale much better with the lateral crack scale factor (${E_1}^{1/2}/H_1$) [Fig. 7(a)] rather than the radial crack scaling factor $[(E_1/H_1{K_{Ic}}^2)^{1/3}]$ [Fig. 7(b)] for the workpiece materials evaluated in this study. The SSD depth increased linearly with ${E_1}^{1/2}/H_1$ up to a value of at least 2 $\text{GPa}^{-1/2}$. CaF_2, which had a high value of ${E_1}^{1/2}/H_1 = 5.8$ $\text{GPa}^{-1/2}$, was the only workpiece material that did not follow the trend.

A possible explanation for why lateral cracks, rather than radial cracks, are correlated to SSD depth is because the lateral cracks are actually deeper than the radial cracks. Consider a single sharp abrasive particle normally loaded via static indentation resulting in both radial and lateral cracks as shown in Fig. 8. Figure 8(a) shows the more commonly drawn schematic where radial cracks are deeper than the lateral cracks, and Fig. 8(b) shows the converse where lateral cracks are deeper.

The analysis below evaluates whether it is possible for the lateral cracks to be deeper than the radial cracks. Using the previously measured values for s_r or s_ℓ,[11] we find that the two are correlated [see Fig. 9(b)], which can be described empirically as

$$s_\ell = 2.2e^{s_r/10.8}. \tag{2}$$

Intuitively this means that the rate of increase in lateral crack depth gets larger with increase in the rate of increase in radial crack depth. Hence despite the fact that the depth of

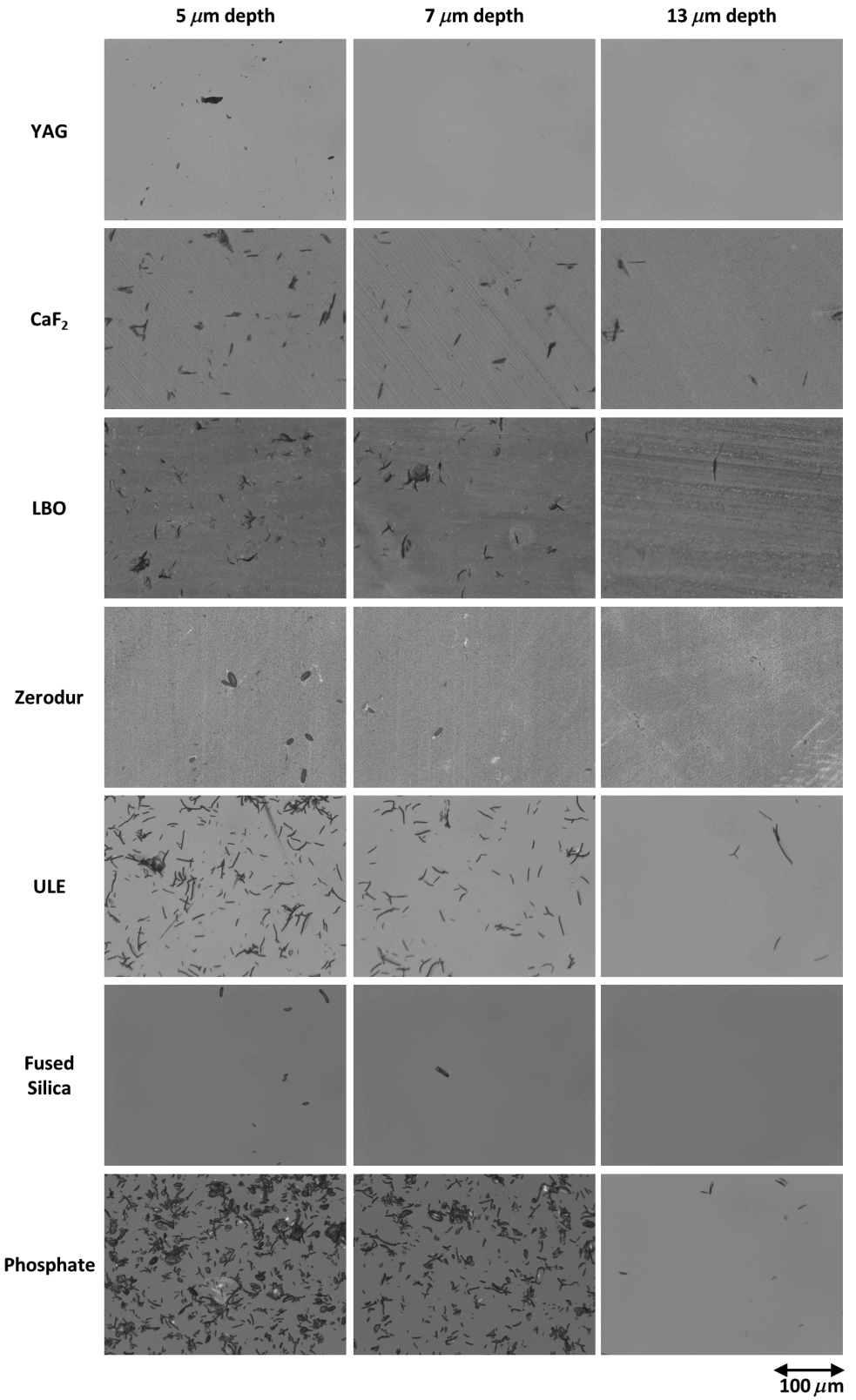

Fig. 4 Optical micrographs of the SSD fractures observed on the various ground workpiece materials after polishing to various depths of 5, 7, and 13 μm and chemically etching ~1 μm using recipe described in Table 1.

radial cracks has a stronger load dependence than lateral cracks [see Eqs. (1a) and (1b)], the propensity to have deeper lateral cracks is driven by Eq. (2). Using Eqs. (1a), (1b), and (2), Fig. 9(b) shows the calculated crack depth difference between radial and lateral cracks ($c_r - c_\ell$) as a function of the radial crack slope (s_r) of the workpiece material for the load range expected on abrasive particles during loose abrasive grinding. A negative value for $c_r - c_\ell$ means that

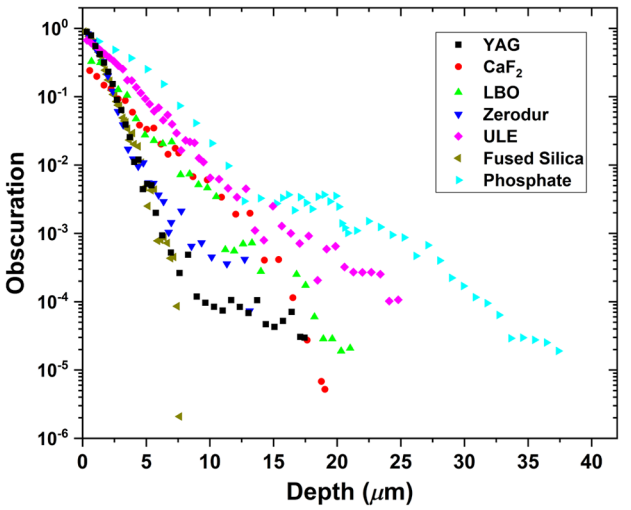

Fig. 5 Measured SSD depth distribution using the MRF wedge technique on various optical materials after a 15-μm Al_2O_3 loose abrasive grind.

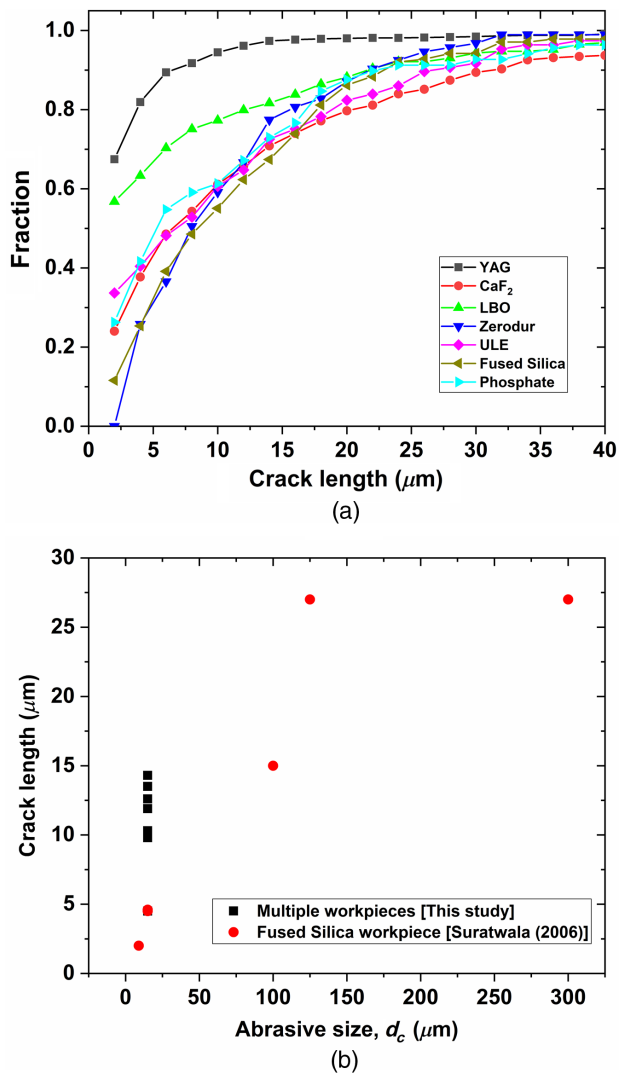

Fig. 6 (a) Measured cumulative crack length distribution using the MRF wedge technique on various optical materials after a 15-μm Al_2O_3 loose abrasive grind and (b) mean crack length versus abrasive size.

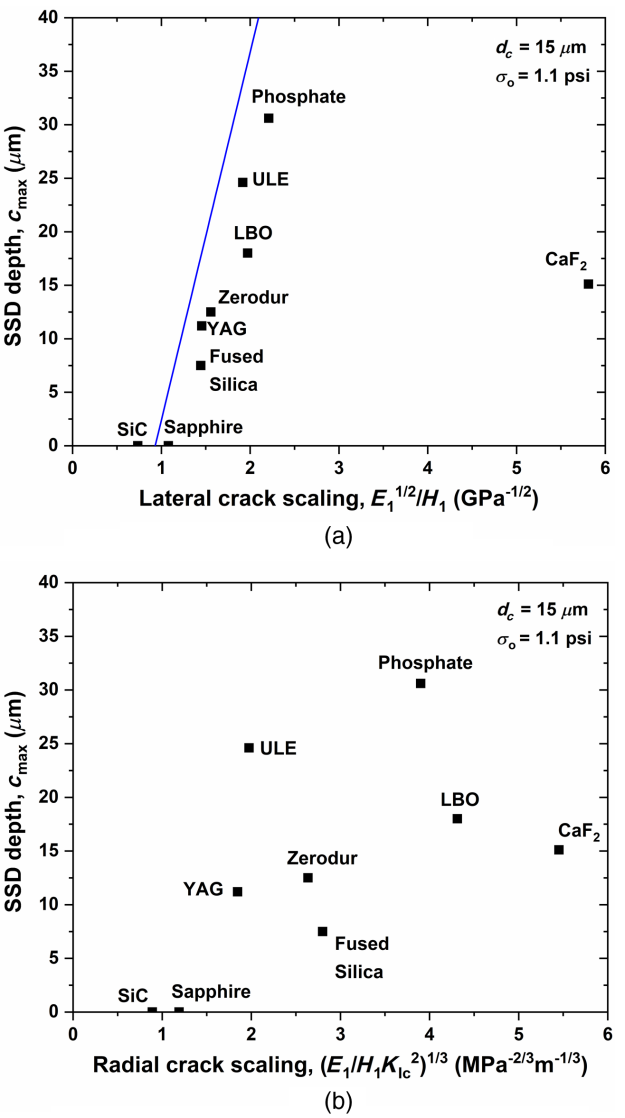

Fig. 7 (a) SSD depth (c_{max}) at 10^{-4} obscuration as a function of workpiece material property scaling for lateral cracks ($E_1^{1/2}/H_1$); (b) SSD depth (c_{max}) at 10^{-4} obscuration as a function of workpiece material property scaling for radial cracks $[(E_1/H_1K_{Ic}^2)^{1/3}]$. The solid line in (a) is that predicted using Eq. (3).

the lateral crack is deeper than the radial crack. The results in Fig. 9(b) suggest that lateral cracks can often be deeper than or nominally equal to the depth of radial cracks in the appropriate load range. This analysis is consistent with the hypothesis that lateral cracks can be deeper than radial cracks, thus explaining why SSD depth was found to scale with the lateral crack depth scaling factor $E_1^{1/2}/H_1$, as opposed to the radial crack depth scaling factor. Note, however, at much higher applied loads, the larger load dependence for the radial cracks would start to dominate resulting in deeper radial cracks, as has been historically described.

4.2 *Prediction of SSD Depth*

As discussed above, the complexity of the grinding process has historically made it challenging to predict SSD depth distributions for various grinding processes and workpiece materials. In this study, the SSD on a broad range of workpiece materials has been measured and evaluated. In a

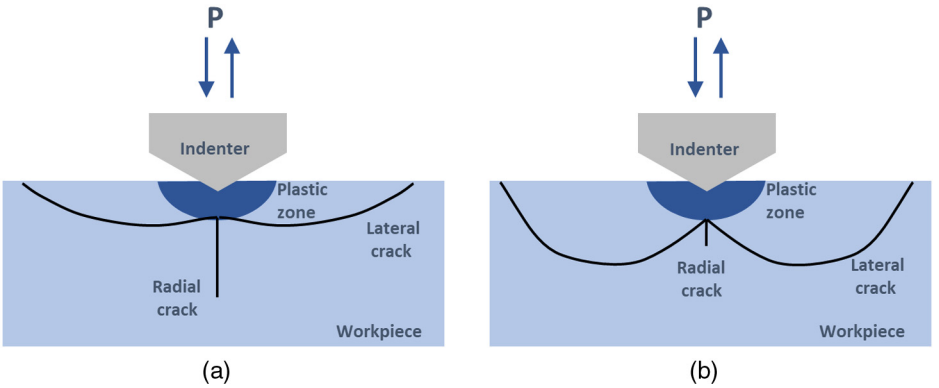

Fig. 8 Schematic illustration of lateral cracks and radial cracks created during static indentation where: (a) radial cracks are deeper than lateral cracks and (b) lateral cracks are deeper than radial cracks.

previous study, the SSD on a broad range of grinding processes on a single workpiece material was measured.[5,6,14] Some of the results of that study as a function of the major grinding process variables (namely abrasive size and applied pressure) are shown in Figs. 10(a) and 10(b). Accounting for the workpiece material scaling to SSD depth described in the previous section [see Fig. 7(a)] and the dependency of SSD depth to applied pressure and abrasive size [see Figs. 10(a) and 10(b)], the following

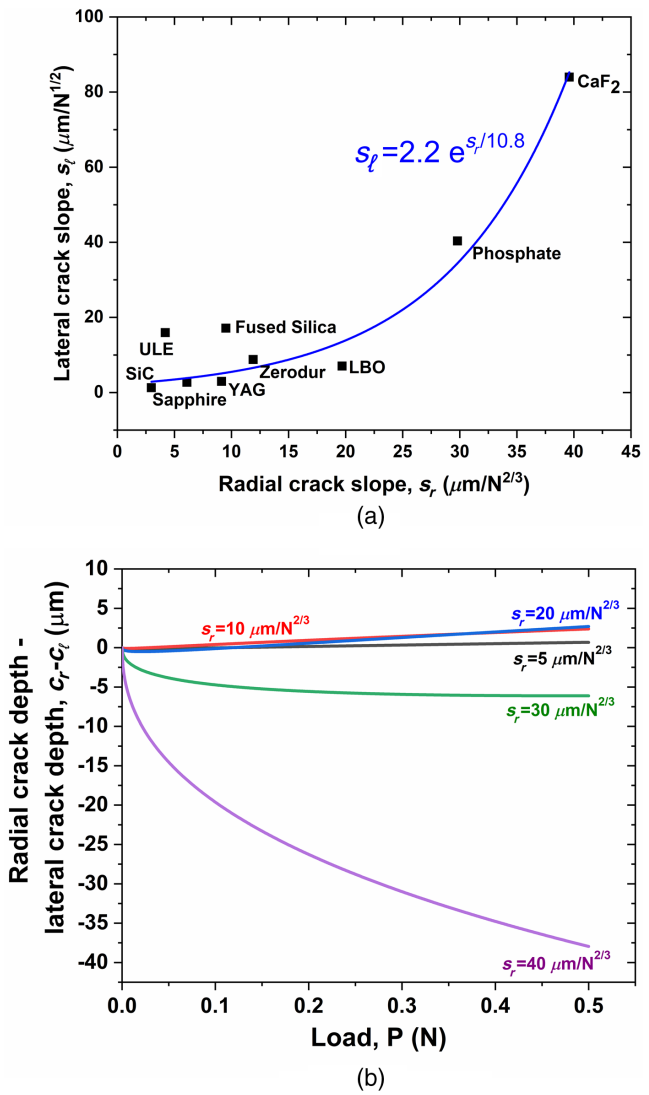

Fig. 9 (a) Correlation between the measured lateral crack slope (s_ℓ) with the radial crack slope for various workpiece materials; (b) calculated difference in radial crack and lateral crack depth as a function of load for workpiece materials with different radial crack growth slopes.

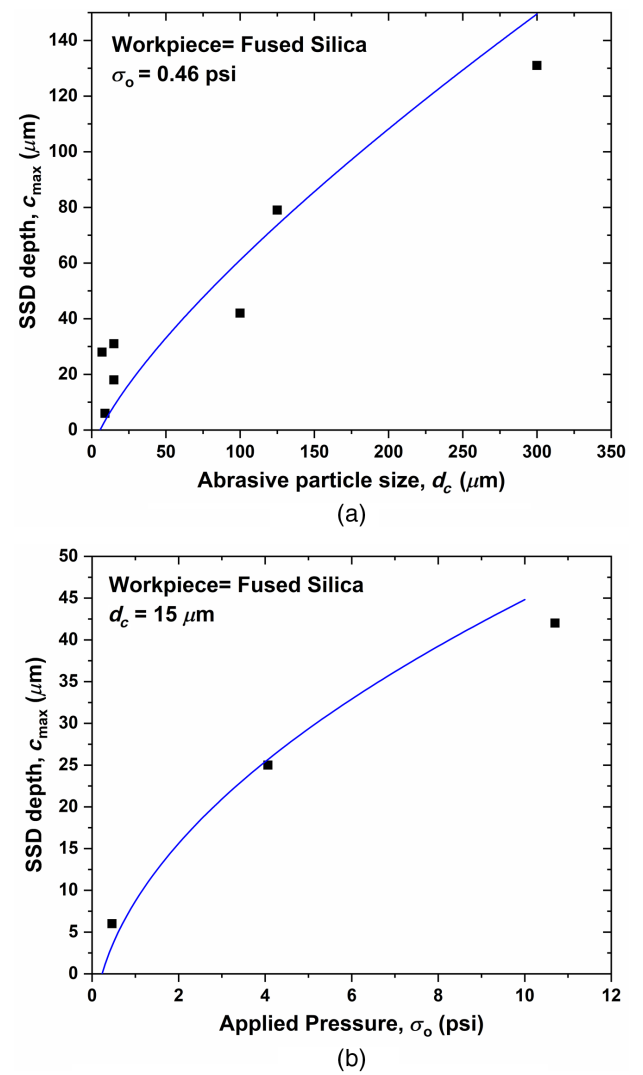

Fig. 10 Measured SSD depth on fused silica workpieces as a function of (a) abrasive size and (b) applied pressure during grinding (data from Refs. 6, 14). The solid lines are those predicted using Eq. (3).

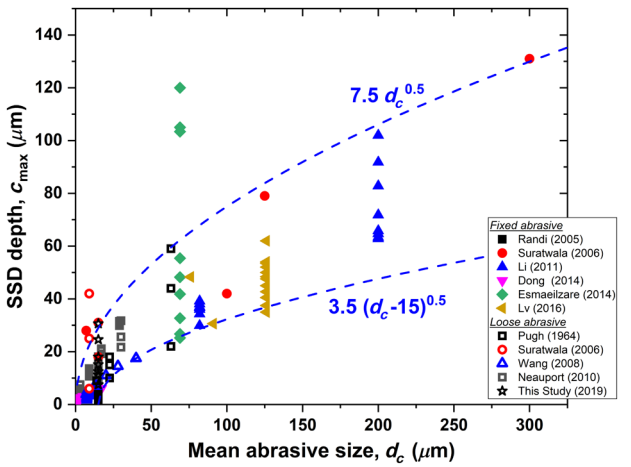

Fig. 11 Measured SSD depth from various studies as a function of grinding abrasive size.[6,15–22]

semiempirical expression can be used to estimate the amount of SSD depth ($c_{\max}$) for standard grinding processes as

$$c_{\max} = \left(\mathrm{C}_a \frac{{E_1}^{1/2}}{H_1} - \mathrm{C}_b\right)\sigma_o^{1/2} d_c^{3/4} - \mathrm{C}_c, \tag{3}$$

where E_1 is the elastic modulus of workpiece (GPa), H_1 is the hardness of workpiece (GPa), σ_o is the applied pressure (psi), and d_c is the mean abrasive particle size (μm) using the constants $C_a = 4.3\ \mu\mathrm{m}^{1/4}\,\mathrm{GPa}^{1/2}\,\mathrm{psi}^{-1/2}$, $C_b = 3.0\ \mu\mathrm{m}^{1/4}\,\mathrm{psi}^{-1/2}$, and $C_c = 8.0\ \mu$m. The solid lines in Figs. 7 and 10 show that Eq. (3) does a reasonable job of describing the expected SSD depth as a function of workpiece material properties, grinding abrasive size, and grinding applied pressure.

To explore how much influence other grinding process variables have on the SSD depth, a broader set of SSD depth data collected on a host of workpiece materials (including those in Table 1, BK7 glass, Si, Ge, InSb, CdTe, and MgF_2) and different grinding processes [including loose and fixed abrasives, different media (Al_2O_3, diamond, SiC), different kinematics or relative velocities, different applied pressures, and different depths of cut for fixed abrasive grinding], measured by a variety of measurement techniques (including MRF wedge, taper polishing, MRF spot, cross sectioning, and roughness change with etching), were evaluated.[6,15–22] Figure 11 summarizes all this data of ~150 measurements plotted as SSD depth as a function of abrasive size. The dominant grinding process variable is the abrasive size that influences the SSD depth, with most of the data falling within the band outlined by the dashed lines. Hence despite all the different grinding process changes described, the SSD depth largely stays within the band shown in Fig. 11.

There are a few points outside the band, which are largely attributed to gross rogue particle contamination leading to an increase in SSD depth. It has been previously shown that rogue particle contamination can significantly increase the SSD depth.[1,6] In other words, the addition of rogue particles effectively increases the abrasive size during grinding resulting in an increase in the load per particle and hence depth of cracking.

The SSD depth band in Fig. 11 can also serve as another useful empirical rule-of-thumb to estimate the range of the amount of SSD that can occur as

$$7.5\ \mu\mathrm{m}^{1/2} d_c^{1/2} \geq c_{\max} \geq 3.5\ \mu\mathrm{m}^{1/2}(d_c - 15\ \mu\mathrm{m})^{1/2} \tag{4}$$

A likely mechanism influencing the lower part of the SSD depth band (i.e., minimum SSD depth for a given abrasive size) is the ductile-to-brittle transition. In other words, lower applied pressures will at some point lead to an inability for fracture to initiate, thus preventing fracture-induced removal. A likely mechanism influencing the upper part of the SSD depth band (i.e., maximum SSD for a given abrasive size) is the maximum depth-of-cut that can be practically implemented during fixed abrasive grinding. This then defines the maximum applied pressure that can result in practical grinding and hence the maximum load per particle leading to fracture and the maximum SSD depth.

5 Conclusions

For a fixed grinding process, we find that SSD depth scales with ${E_1}^{1/2}/H_1$ of the workpiece material being processed. This scaling suggests that lateral cracks are an important and possibly the dominant crack type leading to SSD depth. Combining this workpiece material scaling with previous grinding process-dependent SSD depth correlations, useful semiempirical relationships have been determined to aid in estimating the SSD depth for a given workpiece material and grinding process.

Acknowledgments

This work was performed under the auspices of the U.S. Department of Energy by Lawrence Livermore National Laboratory under Contract DE-AC52-07NA27344 within the LDRD program.

References

1. T. Suratwala, *Materials Science and Technology of Optical Fabrication*, Wiley, Hoboken, New Jersey (2018).
2. Y. Lee, "Evaluating subsurface damage in optical glasses," *J. Eur. Opt. Soc.-Rapid Publ.* **6**, 11001 (2011).
3. T. Suratwala et al., "Partial charge model for predicting material removal rate during chemical polishing," *J. Am. Ceram. Soc.* **102**(4), 1566–1578 (2018).
4. N. Shen et al., "Single particle nanoplastic removal function of optical materials," *J. Am. Ceram. Soc.* 1–11 (2018).
5. J. A. Menapace et al., "MRF applications: measurement of process-dependent subsurface damage in optical materials using the MRF wedge technique," *Proc. SPIE* **5991**, 599103 (2005).
6. T. Suratwala et al., "Sub-surface mechanical damage distributions during grinding of fused silica," *J. Non-Cryst. Solids* **352**(52–54), 5601–5617 (2006).
7. G. Spierings, "Wet chemical etching of silicate-glasses in hydrofluoric-acid based solutions," *J. Mater. Sci.* **28**(23), 6261–6273 (1993).
8. B. R. Lawn, *Fracture of Brittle Solids*, 2nd ed., Cambridge University Press, Cambridge, New York, 378 p (1993).
9. B. Lawn and R. Wilshaw, "Indentation fracture: principles and applications," *J. Mater. Sci.* **10**(6), 1049–1081 (1975).
10. I. M. Hutchings, *Tribology: Friction and Wear of Engineering Materials*, CRC Press, Boca Raton, 273 p (1992).
11. T. Suratwala et al., "Towards predicting removal rate and roughness during grinding of optical materials," *Appl. Opt.* **58**(10), 2490–2499 (2019).
12. J. C. Lambropoulos, S. Xu, and T. Fang, "Loose abrasive lapping hardness of optical glasses and its interpretation," *Appl. Opt.* **36**(7), 1501–1516 (1997).
13. J. C. Lambropoulos et al., "Surface microroughness of optical glasses under deterministic microgrinding," *Appl. Opt.* **35**(22), 4448–4462 (1996).
14. P. E. Miller et al., "The distribution of subsurface damage in fused silica," *Proc. SPIE* **5991**, 599101 (2005).

15. J. A. Randi, J. C. Lambropoulos, and S. D. Jacobs, "Subsurface damage in some single crystalline optical materials," *Appl. Opt.* **44**(12), 2241–2249 (2005).
16. Y. Li et al., "Morphology and distribution of subsurface damage in optical fused silica parts: bound-abrasive grinding," *Appl. Surf. Sci.* **257**(6), 2066–2073 (2011).
17. Z. Dong and H. Cheng, "Study on removal mechanism and removal characters for SiC and fused silica by fixed abrasive diamond pellets," *Int. J. Mach. Tools Manuf.* **85**, 1–13 (2014).
18. A. Esmaeilzare, A. Rahimi, and S. Rezaei, "Investigation of subsurface damages and surface roughness in grinding process of Zerodur® glass-ceramic," *Appl. Surf. Sci.* **313**, 67–75 (2014).
19. D. Lv et al., "Subsurface damage depth and distribution in rotary ultrasonic machining and conventional grinding of glass BK7," *Int. J. Adv. Manuf. Technol.* **86**, 2361–2371 (2016).
20. Z. Wang et al., "Subsurface damage distribution in the lapping process," *Appl. Opt.* **47**(10), 1417–1426 (2008).
21. J. Neauport et al., "Loose abrasive slurries for optical glass lapping," *Appl. Opt.* **49**(30), 5736–5745 (2010).
22. E. Pugh and L. Samuels, "Damaged layers in abraded silicon surfaces," *J. Electrochem. Soc.* **111**(12), 1429–1431 (1964).

Tayyab I. Suratwala is the program director for Optics and Materials Science and Technology at Lawrence Livermore National Laboratory (LLNL). He received his BS degree in ceramic engineering from the University of Illinois at Urbana-Champaign in 1992 and his PhD in materials science and engineering from the University of Arizona in 1996. He has more than 90 peer-reviewed publications, including six patents/patent applications, four R&D100 awards, and a book titled *Materials Science & Technology of Optical Fabrication*. He is a fellow of the Optical Society of America.

William A. Steele: Biography is not available.

Lana L. Wong is a scientist in the Optics and Materials Science and Technology Group at LLNL. She received her BS degree in ceramic engineering in 1986 and her MS degree in materials science and engineering in 1988, both from the University of Washington. Her research interests include finishing (subsurface damage) including slurry stabilization to prevent agglomeration during polishing and etching/mitigation strategies to reduce/eliminate laser-induced damage on NIF optics by improving surface quality.

Gary C. Tham is the optical fabrication technical associate for the Optics and Materials Science and Technology Group at LLNL. He is a veteran of the United States Marine Corps. He earned his BS degree in mechanical engineering from San Jose State University in 1992. Prior to LLNL, he created polish manufacturing processes for the magnetic media industry which saved substantial operating costs through optimization and yield improvements. His current research interest is magnetorheological finishing (MRF).

Joel F. Destino is currently an assistant professor in the Chemistry Department at Creighton University. He received his BS degree in chemistry from Syracuse University in 2008 and his PhD in chemistry from the University at Buffalo in 2016. In 2016, he joined the Optics and Materials Science and Technology group at LLNL as postdoctoral staff. At LLNL, his interests centered on the chemistry of optical materials, including the development of sol-gel feedstocks for fabricating 3D printable optics.

Philip E. Miller is a chemist in the Materials Science Division, at LLNL and has been involved in the laser program at LLNL since 1987. He received his BA degree in chemistry from the California State University at San Bernardino in 1979 and his PhD in chemistry from the University of Arizona in 1985. His research interests include optical fabrication, precursors of laser damage, whole optic migration of laser damage precursors, fracture of brittle materials, and materials characterization.

Nathan J. Ray received his BS degrees in both mathematics and physics from the University of Texas at San Antonio in 2012 and his PhD in materials engineering from the University of Illinois at Chicago in 2017. His research interests include dewetting behavior of thin films, generation of metasurfaces and characterization of their optomechanical properties, fracture behavior in glasses and ceramics, thermally induced glass removal and reflow, plasma electrolytic oxidation, and charge transport across barrier layer nanocomposite systems.

Joseph A. Menapace is a group leader for optical finishing at LLNL. He received his BS degree in chemistry from the United States Air Force Academy in 1982 and his PhD in chemical physics from Colorado State University in 1987. His research includes advanced MRF for optical systems and lasers. He has authored seventy-four publications involving laser optics, high explosives, and supersonic molecular jets. He has four patents involving laser optics, deterministic polishing, and MRF polishing fluids.

Eyal Feigenbaum is a research scientist in the NIF and Photon Science Directorate at LLNL in Livermore. He received his BSc, MSc, and PhD degrees in electrical engineering from the Technion, Israel, in 1998, 2004, and 2008, respectively. Among his current activities are photonics and multiphysics modeling and leading advanced optics research activities. He has more than 40 peer-reviewed publications (mostly as first author) with H-index of 16 and 4 US patent applications.

Nan Shen is a staff physicist in the Materials Science Division of the Physical and Life Sciences Directorate at LLNL. She received her BA degree in physics and applied mathematics from Rhode Island College and her PhD in physics from Harvard University. Her research interests include laser material interaction such as short pulse laser damage in optics and laser machining, as well as deterministic polishing of optical materials.

Michael D. Feit is a theoretical physicist for Optics and Materials Science and Technology at LLNL. He received his BA degree in physics from Lehigh University, Bethlehem, Pennsylvania, in 1964 and his PhD in theoretical physics from Rensselaer Polytechnic Institute, Troy, New York, in 1969. His current research interests include grinding and polishing, deterministic finishing, laser damage initiation and growth, thermal mitigation of laser damage and fracture of glasses. He is a fellow of the American Physical Society and of the Optical Society of America. He has 250 peer-reviewed publications, six patents and two R&D 100 awards.